BIOCHEMISTRY

 Volume 45, Number 39 October 3, 2006

Articles

Interactions of Tryptophan, Tryptophan Peptides, and Tryptophan Alkyl Esters at Curved Membrane Interfaces†

Wei Liu‡ and Martin Caffrey*,‡,§

Department of Chemical and Environmental Sciences and Materials and Surface Science Institute, University of Limerick, Limerick, Ireland, and Biophysics Program, Chemistry Department, The Ohio State University, Columbus, Ohio 43210

Received April 28, 2006; Revised Manuscript Received June 30, 2006

ABSTRACT: Motivated by ongoing efforts to understand the mechanism of membrane protein crystallogenesis and transport in the lipidic cubic phase, the nature of the interaction between tryptophan and the bilayer/aqueous interface of the cubic phase has been investigated. The association was quantified by partitioning measurements that enabled the free energy of interaction to be determined. Temperature-dependent partitioning was used to parse the association free energy change into its enthalpic and entropic components. As has been observed with tryptophan derivatives interacting with glycerophospholipid bilayers in vesicles, tryptophan partitioning in the cubic phase is enthalpy driven. This is in contrast to partitioning into apolar solvents, which exhibits the classic hydrophobic effect whose hallmark is a favorable entropy change. These results with tryptophan are somewhat surprising given the simplicity, homogeneity, and curvature of the interface that prevails in the case of the cubic phase. Nevertheless, the interaction between tryptophan and the mesophase is very slight as revealed by its low partition coefficient. Additional evidence in support of the interaction was obtained by electronic absorption and fluorescence spectroscopy and fluorescence quenching. Partitioning proved insensitive to the lipid composition of the membrane, examined by doping with glycerophospholipids. However, the interaction could be manipulated in meaningful ways by the inclusion in the aqueous medium of salt, glycerol, or urea. The effects seen with tryptophan were amplified rationally when measurements were repeated using tryptophan alkyl esters and with tryptophan peptides of increasing length. These findings are interpreted in the context of the insertion, folding, and function of proteins in membranes.

Diesenhofer and Michel commented on the unexpected nonuniform distribution of tryptophan (W) in the L and M transmembranal subunits of the photosynthetic reaction center (*1*). Since this was the first membrane protein whose high-resolution, 3-D structure had been solved, it provided an unprecedented view of how such a protein was designed to function in a membrane environment. What was unexpected about the distribution was that the bulk of the Ws were located at the ends of transmembranal helices and in connecting helices on the periplasmic side of the protein (*1*). This had the effect of clustering them at the putative interface between the polar aqueous environment and the more apolar interior of the membrane. Since that time, the structures of many membrane proteins have been solved (*2*). With each new addition, the asymmetric distribution of Ws, which has

† Supported in part by Science Foundation Ireland (02-IN1-B266), the National Institutes of Health (GM61070 and GM075915), and the National Science Foundation (DIR9016683 and DBI9981990).

* Corresponding author. Phone: (353) 61-234174; fax: (353) 61-202568; e-mail: martin.caffrey@ul.ie.

‡ The Ohio State University.

§ University of Limerick.

10.1021/bi0608414 CCC: $33.50
Published on Web 09/08/2006

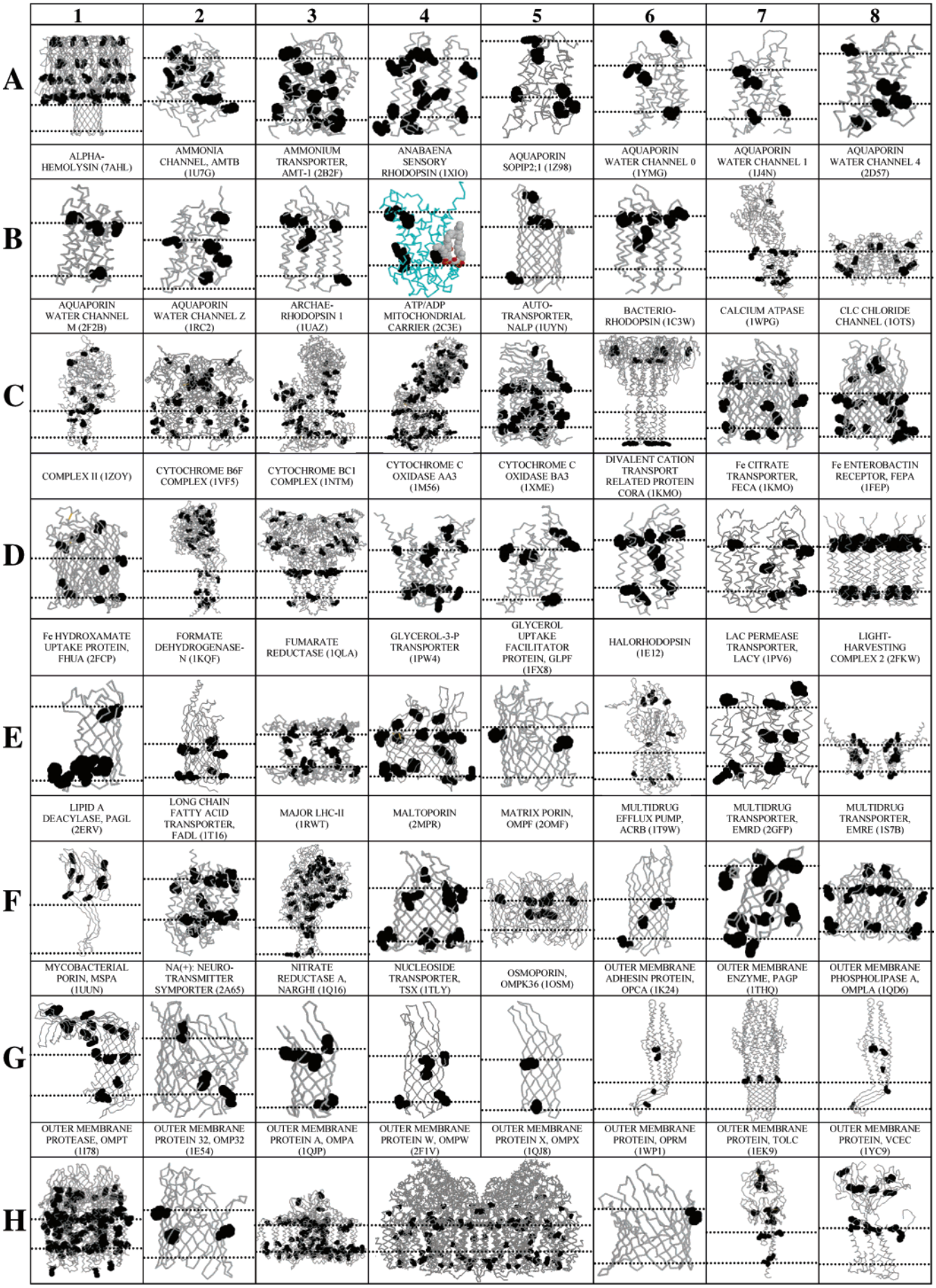
1
2
3
4
5
6
7
8
A
ALPHA-HEMOLYSIN (7AHL)
AMMONIA CHANNEL, AMTB (1U7G)
AMMONIUM TRANSPORTER, AMT-1 (2B2F)
ANABAENA SENSORY RHODOPSIN (1XIO)
AQUAPORIN SOPIP2;1 (1Z98)
AQUAPORIN WATER CHANNEL 0 (1YMG)
AQUAPORIN WATER CHANNEL 1 (1J4N)
AQUAPORIN WATER CHANNEL 4 (2D57)
B
AQUAPORIN WATER CHANNEL M (2F2B)
AQUAPORIN WATER CHANNEL Z (1RC2)
ARCHAE-RHODOPSIN 1 (1UAZ)
ATP/ADP MITOCHONDRIAL CARRIER (2C3E)
AUTO-TRANSPORTER, NALP (1UYN)
BACTERIO-RHODOPSIN (1C3W)
CALCIUM ATPASE (1WPG)
CLC CHLORIDE CHANNEL (1OTS)
C
COMPLEX II (1ZOY)
CYTOCHROME B6F COMPLEX (1VF5)
CYTOCHROME BC1 COMPLEX (1NTM)
CYTOCHROME C OXIDASE AA3 (1M56)
CYTOCHROME C OXIDASE BA3 (1XME)
DIVALENT CATION TRANSPORT RELATED PROTEIN CORA (1KMO)
Fe CITRATE TRANSPORTER, FECA (1KMO)
Fe ENTEROBACTIN RECEPTOR, FEPA (1FEP)
D
Fe HYDROXAMATE UPTAKE PROTEIN, FHUA (2FCP)
FORMATE DEHYDROGENASE-N (1KQF)
FUMARATE REDUCTASE (1QLA)
GLYCEROL-3-P TRANSPORTER (1PW4)
GLYCEROL UPTAKE FACILITATOR PROTEIN, GLPF (1FX8)
HALORHODOPSIN (1E12)
LAC PERMEASE TRANSPORTER, LACY (1PV6)
LIGHT-HARVESTING COMPLEX 2 (2FKW)
E
LIPID A DEACYLASE, PAGL (2ERV)
LONG CHAIN FATTY ACID TRANSPORTER, FADL (1T16)
MAJOR LHC-II (1RWT)
MALTOPORIN (2MPR)
MATRIX PORIN, OMPF (2OMF)
MULTIDRUG EFFLUX PUMP, ACRB (1T9W)
MULTIDRUG TRANSPORTER, EMRD (2GFP)
MULTIDRUG TRANSPORTER, EMRE (1S7B)
F
MYCOBACTERIAL PORIN, MSPA (1UUN)
NA(+): NEURO-TRANSMITTER SYMPORTER (2A65)
NITRATE REDUCTASE A, NARGHI (1Q16)
NUCLEOSIDE TRANSPORTER, TSX (1TLY)
OSMOPORIN, OMPK36 (1OSM)
OUTER MEMBRANE ADHESIN PROTEIN, OPCA (1K24)
OUTER MEMBRANE ENZYME, PAGP (1THQ)
OUTER MEMBRANE PHOSPHOLIPASE A, OMPLA (1QD6)
G
OUTER MEMBRANE PROTEASE, OMPT (1I78)
OUTER MEMBRANE PROTEIN 32, OMP32 (1E54)
OUTER MEMBRANE PROTEIN A, OMPA (1QJP)
OUTER MEMBRANE PROTEIN W, OMPW (2F1V)
OUTER MEMBRANE PROTEIN X, OMPX (1QJ8)
OUTER MEMBRANE PROTEIN, OPRM (1WP1)
OUTER MEMBRANE PROTEIN, TOLC (1EK9)
OUTER MEMBRANE PROTEIN, VCEC (1YC9)
H

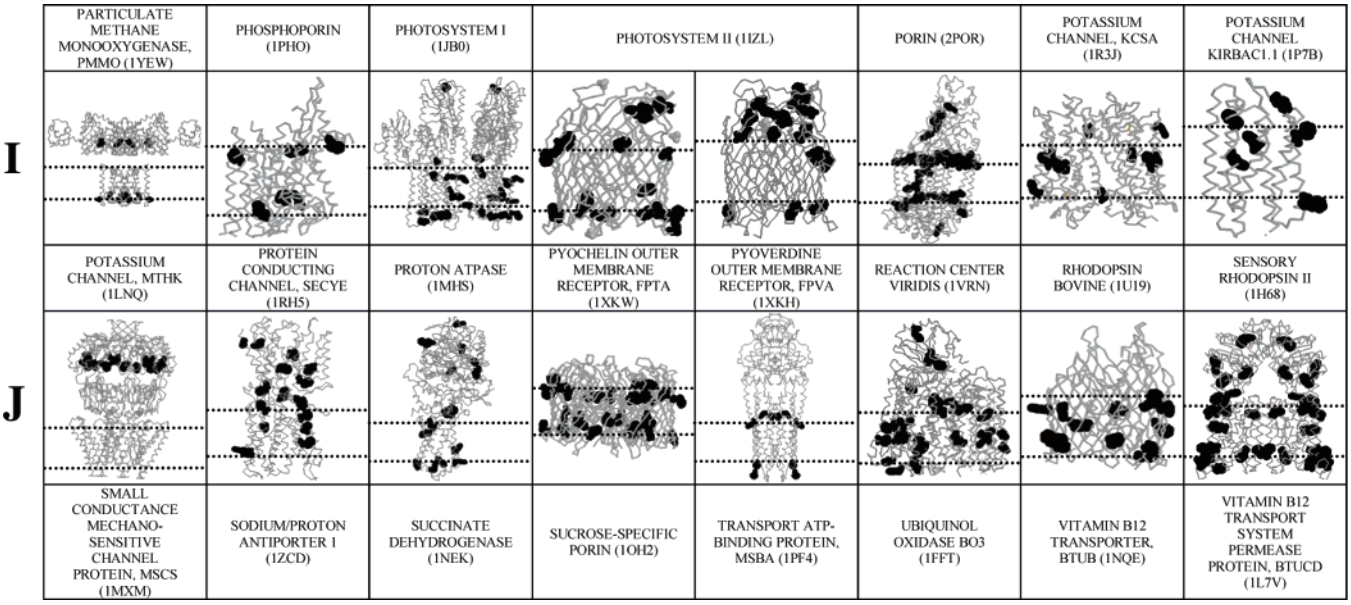

FIGURE 1: Distribution of tryptophans in integral membrane proteins of known structure. The proteins included in the figure were selected from the unique protein family subset in the Membrane Protein Data Bank (ref 2, http://www.mpdb.ul.ie). The C_α-backbone trace of the protein is shown in gray (cyan in the case of 2C3E, panel B4), while the tryptophans are represented as black space-filling spheres. Proteins are arranged alphabetically by name and abbreviated in the interest of space, and the PDB accession number is given. The dotted lines show the approximate location of the membrane/aqueous interfaces and are ~30 Å apart. Positioning of proteins in the membrane is based on the original literature or a best guess by the authors. Models have been scaled to fit the panel. No particular vectoral orientation of proteins across the membrane has been imposed other than generally to place the bulkier extramembranal domain in the upper part of each panel. The view of the protein model shown was chosen to optimize visualizing the distribution of tryptophans in the vicinity of the interface. In the interest of space, only truly unique membrane protein structures are shown. Thus, for example, the photosynthetic reaction center from *Blastochloris* (*Rps.*) *viridis* is included in the figure while that from *R. sphaeroides* is not. The following proteins do not contain tryptophans and were omitted from the figure in the interest of space: ATP synthase (1QO1); glutamate transporter homologue (1XFH); large conductance mechanosensitive channel, MSCL (1MSL); outer membrane protein, NSPA (1P4T); sodium ATPase, F-type (1YCE); and sodium ATPase, V-type (2BL2). In panel B4, a single cardiolipin molecule is shown in space-filling form with the following atom type coloring scheme: carbon, gray; oxygen, red; and phosphorus, orange.

now been extended to include tyrosine, is looked for. With some regularity, the fingerprint is seen (Figure 1). However, there are exceptions as in the case of the lumenal side of the calcium-ATPase from sarcoplasmic reticulum (*3*).

In support of this nonuniform distribution of Ws in integral membrane proteins, a number of systematic studies have been carried out to investigate the propensity of the different amino acids for the membrane environment. Most of the work has been done using glycerophospholipid vesicles as model membranes. The data thus far are consistent with W, showing a definite preference for the polar/apolar interface (*4*−*8*). However, the exact nature of the interaction remains elusive (*5*).

The current study that relates to W/membrane interactions was motivated in part by our interest in understanding the mechanism by which membrane proteins crystallize in the lipidic cubic mesophase (*9*) by the so-called in meso method (reviewed in ref *10*). Crystals so produced are used for structure determination by crystallographic means. The cubic phase can be viewed as a molecular sponge consisting of a curved lipid bilayer that divides the aqueous compartment into two interpenetrating but noncontacting channels (Figure 2). Our working hypothesis posits that the membrane protein reconstitutes into the lipid bilayer of the cubic phase prior to nucleation and crystal growth. Testing the hypothesis requires a characterization of the transport properties of the cubic phase that coincidentally is relevant to other areas of research such as controlled uptake and release (*11*, *12*). In the course of performing these transport studies, some of which were done with W, it was noted that release of this amino acid was biphasic. The first phase was rapid and accounted for ~98% of the incorporated W (*11*). The remainder released but slowly. The data suggested that W partitions into or onto the bilayer of the cubic phase from which it slowly releases. However, these findings were not entirely satisfactory given the very slight degree of partitioning observed. Further, we had not anticipated the effect given the chemical simplicity and homogeneity of the lipidic membrane that constitutes the cubic phase. These are formed from monoolein, a monoacylglycerol with a glycerol headgroup to which an acyl chain is esterified. If W resides in the membrane at the interface, it will be enveloped by the hydroxyls and the methylene and methynes of glycerol and by the ester moiety of the alkyl-to-glycerol linkage.

The purpose of the current study was to examine the nature of the W/membrane interaction in more detail as applied to the cubic phase. Specifically, we set out to quantify the process thermodynamically and to test a series of hypotheses that emerged in the course of the investigation. Thus, while the W/membrane interaction is weak, a hypothesis was advanced that alkylating the amino acid would enhance partitioning. By the same token, if W partitions weakly, then the di- and tripeptides, WW and WWW, should show considerably enhanced binding. Further, if partitioning were happening as envisaged—with the indole ring at the interface and directed into the hydrocarbon interior of the bilayer—it should be possible to quench its intrinsic fluorescence by incorporating a lipid with a quenching moiety in its acyl

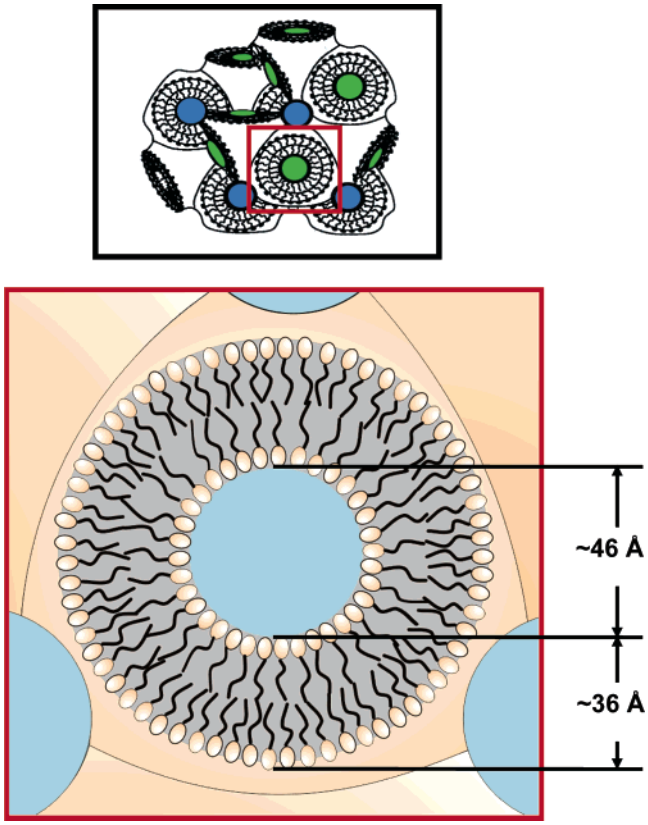

FIGURE 2: Cartoon representation of cubic-*Pn*3*m* phase. Lipids are shown with the glycerol headgroup as an ellipse and the acyl chain as a wavy black line. Aqueous channels are shown in green and blue in the upper panel and in light blue in the lower panel. The phase is drawn to scale and represents that formed by monoolein at 40% (w/w) water and 20 °C (*16*).

chain. The hypotheses have been tested and proven. The results lead to the additional conclusion that the bilayer of the cubic phase, despite its high degree of curvature, is a reasonable model membrane with which to characterize interactions of the type described. Further, the cubic phase offers some distinct advantages for such studies as discussed. The results are examined in light of their relevance to protein interaction with and orientation and function in membranes. Possible uses of the cubic phase as a system in which to reconstitute, refold, and crystallize membrane proteins that begin as inclusion bodies are also discussed.

MATERIALS AND METHODS

Monoolein (MW 356 g/mol, lots M239-JA22-N, M239-MA26-N, and M239-JA12-N) was purchased from Nu Chek Prep Inc. (Elysian, MN). 2,3-Dihydroxypropyl (7*Z*)-9,10-dibromooctadecanoate (bromo-MAG,[1] MW 516 g/mol, 180BR-11 and 180BR-13), dioleoyl phosphatidylcholine (DOPC, MW 786.1 g/mol, lot 180PC-138), dioleoyl phosphatidylethanolamine (DOPE, MW 744.0 g/mol, lot 181PE-159), and *N*-phytanoyl-3-amino-1,2-propanediol (PAL, MW 385.6 g/mol, lot N4ME160APD-10) were obtained from Avanti Polar Lipids Inc. (Alabaster, AL). L-Tryptophan (W, MW 204.2 g/mol, lot 119H0344), dl-tryptophan methyl ester hydrochloride (W−C_1, MW 254.7 g/mol, lot 043H3252), dl-tryptophan ethyl ester hydrochloride (W−C_2, MW 268.7 g/mol, lot 23H0221), and DL-tryptophan butyl ester hydrochloride (W−C_4, MW 296.7 g/mol, lot 99F5013) were purchased from Sigma (St. Louis, MO). Indole (MW 117.1 g/mol, lot 10820KS) was obtained from Aldrich (Milwaukee, WI). The dipeptide tryptophanyl tryptophan (WW, MW 390.4 g/mol, lot 7462E) was obtained from MP Biomedicals Inc. (Irvine, CA), and the tripeptide tryptophanyl tryphanyl tryptophan (WWW, MW 576.7 g/mol, lot 0567590) was from Bachem Bioscience Inc. (King of Prussia, PA). Glycerol (MW 92.1 g/mol, lot 970742), potassium chloride (MW 74.6 g/mol, lot 027298), and urea (MW 60.1 g/mol, lot 015880) were from Fisher Scientific (Pittsburgh, PA). Ruthenium-tris(2,2′-bipyridyl) dichloride (rubipy, MW 748.6 g/mol) was kindly provided by Prof. Claudia Turro (The Ohio State University). Sodium potassium phosphate was from Fluka (Buchs, SG, Switzerland). For the thin-layer chromatography work, solvents of analytical grade from Fisher Scientific (Pittsburgh, PA) were used. Quartz cuvettes (0.01, 0.1, 1, and 3 mm path length) were from Hellma International (Plainview, NY). Syringes were from Fisher Scientific (Hamilton 81030, 100 μL gastight). Water, with a resistivity of >18 MΩ cm, was purified by using a Milli-Q Water System (Millipore Corporation, Bedford, MA) consisting of a carbon filter cartridge, two ion-exchange filter cartridges, an organic removal cartridge, and a final 0.2 μm filter (Sterile Millipore, Millipak 40, lot F2PN84024).

Sample Preparation. Cubic Phase Samples. All samples were prepared at room temperature (20−24 °C). For the bulk of the studies, 25 mM sodium potassium phosphate buffer, pH 5.60 (SPP) was used as the dispersing lyotrope. As needed, the SPP buffer included members of the tryptophan peptide (W_n) or tryptophan alkyl ester (W−C_n) series of additives at a concentration of ≤3 mM. Lipids were removed from the freezer at −70 °C and thawed at room temperature (bromo-MAG) or 40 °C (monoolein). Molten lipid was transferred to a syringe mixing device, and the cubic phase was prepared by mechanical homogenization following published procedures (*13*, *14*). To obtain optically clear samples for spectroscopic measurements, the sample composition was adjusted to ensure formation of a pure cubic-*Pn*3*m* phase. The actual compositions of the samples used in this study are as follows: 40% (w/w) SPP for monoolein (*15*, *16*) and 35% (w/w) SPP for bromo-MAG (unpublished data). Mixed lipid samples were prepared as described previously (*11*, *17*).

To verify that the mesophase sought was actually obtained, aliquots of the above samples were sealed in 1 mm quartz X-ray capillaries and used in X-ray diffraction measurements, as described below.

Spectroscopic Measurements. UV−Vis Absorption. Spectra were recorded with a Uvikon XL dual beam spectrophotometer (Research Instruments International., San Diego, CA), as described (*18*). Data were collected in the range from 750 to 250 nm in 1 nm steps at 100 nm/min with air as the reference. The absorption spectrum of a lipid/SPP buffer dispersion or SPP buffer alone in a quartz cuvette (Hellma) of suitable path length recorded against air was subtracted from sample spectra as appropriate.

[1] Abbreviations: Bromo-MAG, 2,3-dihydroxypropyl (7*Z*)-9,10-dibromooctadecanoate; MPDB, The Membrane Protein Data Bank; W_n, tryptophan peptide series where *n* is the number of tryptophans; W−C_n, tryptophan alkyl ester series where *n* is the number of carbons in the alkyl chain.

Fluorescence. Emission spectra were recorded using an SFM3 fluorimeter (Bio-Logic Science Instruments, Claix, France) that included a 150-Watt Hg/Xe lamp (L2482, Hamamatsu, Japan) and Jobin Yvon monochromators (MM-200 driving unit, BH10 UV monochromators), as described (*18*). One millimeter slits were placed at the entrances to and exits from the excitation and emission monochromators, providing an 8 nm band-pass. The 305 nm light was used for excitation,[2] and emission data were collected from 360 to 320 nm (1 nm steps, 100 nm/min). Light intensity was measured with a photomultiplier tube (Bio-Logic PMT 200) and an integration time of 100 ms.

When the sample absorption exceeded 0.1, the fluorescence intensity no longer rose linearly with concentration. A correction for this so-called inner filter effect has been applied to all relevant data following established procedures (*19*), as described (*18*).

Release Experiments. The additive-loaded cubic phase was transferred to a home-built sample holder (outer diameter, 7.8 mm; thickness, 0.68 mm; sample-holding volume, ~30 μL; exposed sample surface area, 0.48 cm^2), as described (*11*). A spatula was used to fill the holder with the cubic phase and to produce a uniformly flat, exposed surface. At the point of loading, a small aliquot of the cubic phase sample was taken and analyzed by X-ray diffraction for phase identification and microstructure characterization. The initial additive content of the cubic phase was calculated by knowing the concentration of the additive solution used to prepare the cubic phase and the weight of the cubic phase in the sample holder.

To quantify the release of additives from the cubic phase, a multicompartment dialysis cell was used. It has two compartment types: the source, corresponding to the cubic phase sample holder (described previously) and the sink, consisting of a chamber with 1 mL of buffer. The two compartments are separated by a dialysis membrane (mixed cellulose esters, 110 μm thick, 8 μm pore size; lot H2AN07696, Millipore Corp., Bedford, MA). Each experiment made use of a reference sample cell (cubic phase only) and triplicate sample cells (additive-loaded cubic phase). Throughout the experiments, the dialysis cells were shaken gently on a Mistral Multi-Mixer (Lab-Line Instruments Inc., Melrose Park, IL) in an incubator (Model 815, Precision Scientific Inc., Chicago, IL) at 20 °C. A measurement consisted of removing the entire 1 mL solution from the sink and immediately replenishing it with 1 mL of fresh buffer. The concentration of additive in the sink solution was determined by measuring the absorbance at 280 nm (cell path length 1 cm, calibrated with standards of known concentration and measured absorbtivity values of 5600 M^{-1} cm^{-1} for W, W$-C_1$, W$-C_2$, and W$-C_4$, 10 540 M^{-1} cm^{-1} for WW, and 15 310 M^{-1} cm^{-1} for WWW) in a UV−vis spectrophotometer (Uvikon XL). Measurements were made at timed intervals for up to 4 days. The results are reported as the fraction of additive released versus time. At the end of the release experiments, the dialysis cells were taken apart, and the lipid dispersion was sampled for phase characterization by X-ray diffraction. The aqueous content of the lipid dispersions at the end of the release study was determined gravimetrically using a microbalance (R200D, Sartorius Corp., Edgewood, NY) (*13*). The additive release profiles can be described by a Fickian model. A complete evaluation of this model and its use in obtaining diffusion coefficients and partitioning rate constants has been presented (*11*).

Partition Coefficient. The distribution of tryptophan and peptides between the lipid bilayer and the aqueous compartment of the cubic phase at equilibrium was determined experimentally as a partition coefficient (P_χ). P_χ is defined in mole fraction units (*8*, *20*) as

$$P_\chi = \frac{X_{\text{bilayer}}}{X_{\text{aqueous}}} = \frac{[\text{A}]_{\text{bilayer}}}{[\text{A}]_{\text{aqueous}}} \frac{\nu_{\text{bilayer}}}{\nu_{\text{aqueous}}} \quad (1)$$

where X_{bilayer} and X_{aqueous} are the mole fractions of additive in the cubic phase bilayer and the aqueous channel compartments, respectively, $[\text{A}]_{\text{bilayer}}$ and $[\text{A}]_{\text{aqueous}}$ are the molar additive concentrations in the cubic phase bilayer and aqueous channel compartments, respectively, and $\upsilon_{\text{bilayer}}$ and $\upsilon_{\text{aqueous}}$ are the partial molecular volumes of lipid (~629 Å^3) and water (~30 Å^3), respectively.[3] P_χ was measured by incubating together the additive solution and a bolus of cubic phase and following a net loss of additive to the bolus indicating a preferential partitioning into the mesophase. Measurements were carried out in semi-micro, UV-transparent, disposable cuvettes (path length 1 cm; BrandTech Scientific, Essex, CT) such that the concentration of additive in the aqueous medium above the cubic phase could be monitored directly in situ. The cubic phase (~40% (w/w) buffer) was prepared as stated previously, and a known amount (~30 mg) was placed in the bottom of the cuvette. To this was added 1 mL of additive solution (typically 0.30 mM W, 0.15 mM WW, and 0.10 mM WWW), and the cuvettes were capped and sealed with Parafilm. Throughout the equilibration, samples were shaken gently (Mistral Multi-Mixer) in an incubator at 20 °C in the dark. Periodically, cuvettes were transferred to the Uvikon spectrophotometer where the absorption spectrum from 400 to 250 nm of the aqueous solution above the cubic phase was recorded. Absorption at 280 nm was used to calculate the additive concentration, as noted previously. Equilibrium was reached in ≤4 days. All samples were prepared in triplicate. Controls were run that were devoid of the additive and/or cubic phase. For partition measurements performed at other than 20 °C, the aqueous solution above the cubic phase was removed from the sample, and its absorbance was recorded at room temperature. Temperature-dependent partitioning data were processed using the Gibbs free energy equation

$$\Delta G = \Delta H - T\Delta S = -RT \ln P_{\text{x}} \quad (2)$$

where ΔG, ΔH, and ΔS refer, respectively, to the change in free energy, enthalpy, and entropy, R is the gas constant, and T is temperature (Kelvin). Thus, a plot of ΔG versus T provides $-\Delta S$ from the slope and ΔH from the vertical intercept.

[2] 280 nm is the wavelength commonly used to excite W fluorescence. However, due to strong lipid absorption there, the longer wavelength of 305 nm was used instead. See ref *18* for more details.

[3] Molecular volumes were calculated using the known density of water, 0.998 g/mL, and monoolein, 0.942 g/mL, at 20 °C (*21*) and the corresponding molecular weights (18.02 g/mol, water and 356.54 g/mol, monoolein). The values of $\upsilon_{\text{bilayer}}$ and $\upsilon_{\text{aqueous}}$ change by less than 1% in the temperature range from 20 to 40 °C (data not shown).

To calculate P_χ according to eq 1, it is assumed that the previous measurement of additive concentration in the aqueous medium in equilibrium with the cubic phase is also a measure of $[A]_{aqueous}$ and that water inside the cubic phase has the same characteristics as that in the bulk aqueous medium. $[A]_{bilayer}$ was determined by mass balance.

The aqueous content of the fully hydrated cubic phase is sensitive to temperature (Figure S1) and to certain additives. This limiting hydration value, which is used in calculating P_χ, was determined by monitoring the phase state of the dispersion. Pure lipid or aqueous medium were added incrementally and gravimetrically until the boundary was found. The composition where this occurred was used in subsequent calculations.

To demonstrate that additive partitioning is a reversible process, the following experiment was carried out. At the end of a partitioning study when the system had reached equilibrium, the aqueous solution above the cubic phase was removed and was replaced with 0.5 mL of SPP buffer. Release of bound additive into the fresh, additive-free buffer with time was followed spectroscopically in situ, as stated previously.

X-ray Diffraction. Phase characterization was carried out using low- and wide-angle X-ray diffraction in 1 mm diameter quartz capillaries (Hampton Research, Laguna Niguel, CA), as described (*18*). Measurements were performed under controlled temperature conditions with a stability of ±0.05 °C. A typical exposure time was 30 min. Diffraction pattern registration on high-resolution image plates and subsequent analyses has been described (*22*).

RESULTS

Phase Behavior. Throughout this study, monoolein was the primary lipid used to form the cubic phase. Without exception, experiments were performed using the cubic phase with a space group designation, *Pn*3*m*, established by small-angle X-ray diffraction (see ref *23*). Since phase behavior is sensitive to composition (*16*), it was necessary to establish the amounts of the various additives (W_n, $W-C_n$, KCl/Br, glycerol, urea, and glycerophospholipids) used in the study that can be tolerated by the phase. This too was ascertained by small-angle X-ray diffraction. For most additives, phase identity and microstructure were monitored as a function of loading. The cubic-*Pn*3*m* phase was found to be quite forgiving in that sizable amounts of additives were accommodated. However, beyond some limit, the phase became unstable and transformed to or coexisted with another. These limits have been established, and the corresponding data are presented in Tables S1−S5. All of the work reported herein was performed under conditions where the cubic-*Pn*3*m* phase was stable.

Spectroscopic Behavior. In Aquo. As a prelude to documenting the spectroscopic properties of the W_n and $W-C_n$ series of additives in the cubic phase, their spectroscopic behavior in aqueous solution will be described. Thus, the UV spectrum of the $W-C_n$ series is shown in Figure S2A. They are superimposable with no detectable effect of ester bond formation or of alkyl chain length on electronic absorption. In contrast, the absorbtivity of members of the W_n series dropped progressively by ~10% as *n* rose from 1 to 3 (Figure S2B). The absorption profile itself, however, was unaffected by the number of Ws in the range studied.

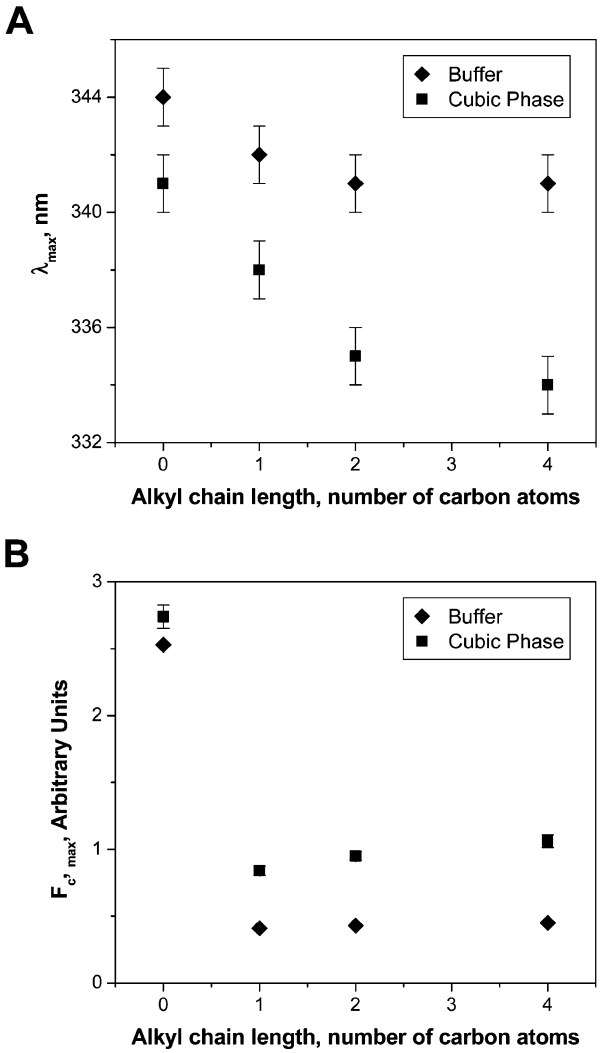

FIGURE 3: Fluorescence characteristics of tryptophan and its alkyl ester derivatives in SPP buffer and in cubic-*Pn*3*m* phase of hydrated monoolein at 20 °C. λ_{max} (A) and $F_{c,max}$ (B) are the wavelength and corrected intensity of maximum fluorescence emission. Data are shown as the average of at least three replicate sample preparation and fluorescence measurements. Error bars correspond to the standard deviation. Occasionally, the statistical error is smaller than the size of the symbol.

The effects of W modification on the fluorescence emission properties of the additives are documented in Figure S2. W alone in aquo has a fluorescence maximum at 344 nm.[4] Upon alkylation, the maximum intensity dropped by a factor of ~5 and was accompanied by a very slight blue shift to 341−342 nm. However, the effects were not dependent on alkyl chain length in the range studied. The W_n series exhibited a similar response in that the fluorescence intensity maximum was reduced by severalfold upon peptide formation and extension with W (Figure S2B). In this case, however, a slight (1−2 nm) red shift was observed. Combined, these data suggest that modification of the α-carboxyl group of W with either an ester or an amide linkage is responsible for the attenuation of fluorescence

[4] This wavelength is a little on the low side since, according to Lakowicz (*19*), W has an emission maximum at 348 nm in water. However, the actual value depends very much on the polarity of the medium in which W is dispersed and on the transmission properties of the optics in the instrument used to make the measurement. The wavelength values reported herein have not been corrected in any way.

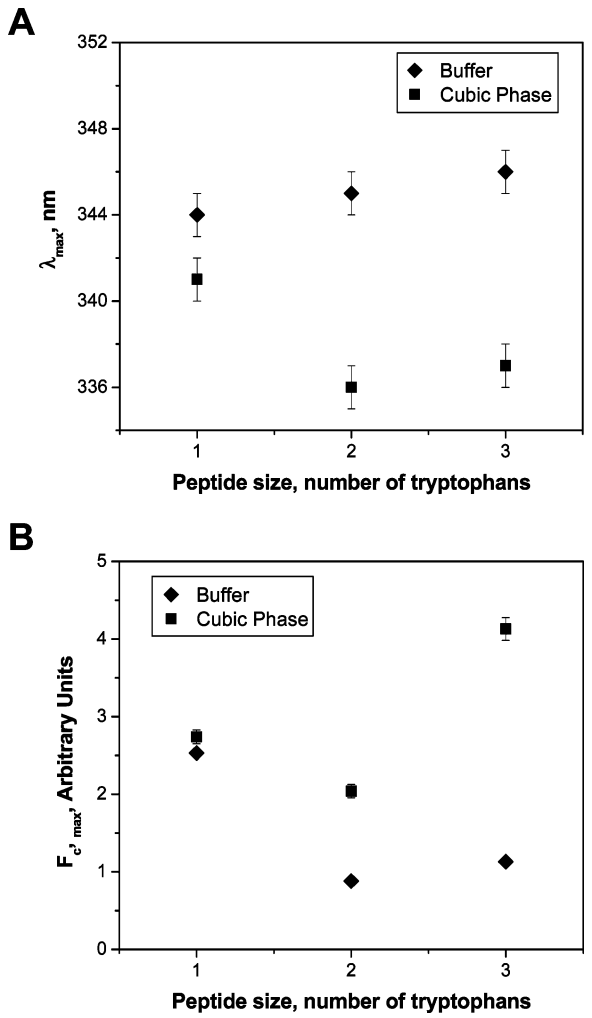

FIGURE 4: Fluorescence characteristics of tryptophan peptides in SPP buffer and in the cubic-*Pn*3*m* phase of hydrated monoolein at 20 °C. λ_{max} (A) and $F_{c,max}$ (B) are the wavelength and corrected intensity of maximum fluorescence emission. Data are shown as the average of at least three replicate sample preparation and fluorescence measurements. Error bars correspond to the standard deviation. Occasionally, the statistical error is smaller than the size of the symbol.

emission observed with this aromatic amino acid, as observed previously (*24*).

Cubic Phase Effects. The UV absorption properties of W proved relatively insensitive to whether the amino acid was in a bulk aqueous solution or was dispersed in the lipidic cubic phase (data not shown). The absorbtivity value at λ_{max} was not affected significantly, and λ_{max} underwent at most a 2 nm red shift from 279 nm upon dispersion in the cubic phase. The red shift suggests that the environment of the W changed slightly upon mesophase incorporation. Identical behavior was observed with other members of the W_n and $W-C_n$ series (data not shown).

In contrast, the fluorescence properties of the W series of additives proved quite sensitive to cubic phase incorporation. Thus, W alone was found to undergo a 3 nm blue shift from 344 nm (Figure 3A) and an 8% increase in fluorescence yield (Figure 3B). Both effects are consistent with a more hydrophobic environment for the amino acid in the cubic phase.

One of the hypotheses being tested in this study was that W-alkylation would serve to anchor it in the bilayer of the cubic phase and that the W headgroup of the alkylated

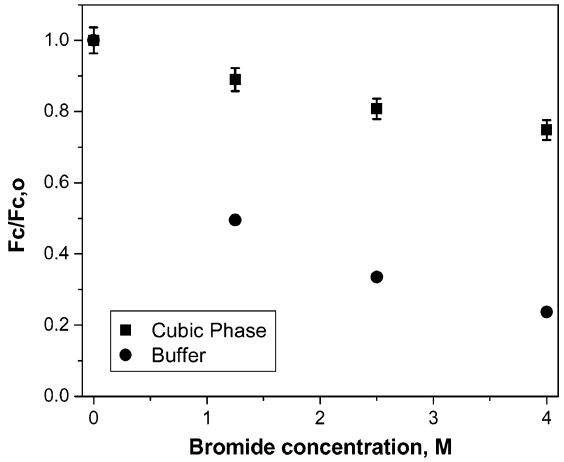

FIGURE 5: Accessibility of tryptophan in SPP buffer and in the cubic-*Pn*3*m* phase of monoolein at 20 °C to the water-soluble quencher, bromide, as judged by fluorescence quenching. Bromide concentration refers to the potassium bromide concentration in the water channels of the cubic phase. Fluorescence data have been corrected for background fluorescence from buffer and lipid and for the inner filter effect and have been normalized to the quencher-free ($F_{c,0}$) value. Data are shown as the average of at least three replicate sample preparations and fluorescence measurements. Error bars correspond to the standard deviation. Occasionally, the statistical error is smaller than the size of the symbol. Stern−Volmer analysis (ref *25*) has been applied to the quenching of tryptophan in SPP buffer. The corresponding plot of $F_{c,0}/F_c$ vs bromide concentration is linear in the range examined with a correlation coefficient of 0.99 and a Stern−Volmer quenching constant of 0.80 M^{-1}. An analysis of quenching behavior in the more complex cubic phase system was not undertaken in this study (see also Figure 6 caption).

additive would experience an increasingly hydrophobic environment as the chain length increased. The data shown in Figure 3 support the hypothesis. Thus, the blue shift increased from 3 nm for W to 4, 6, and 8 nm for $W-C_1$, $W-C_2$, and $W-C_4$, respectively, upon transfer to the cubic phase (Figure 3A). The corresponding increases in fluorescence yields were 204, 220, and 236% (Figure 3B).

Another hypothesis under investigation was that adding more Ws to W in the W_n series would render the peptide more interface-loving and that the effect should reveal itself by reflecting a more hydrophobic environment. This is precisely what was observed. The data in Figure 4 show that extending W to WW and WWW brought about blue shifts of ~9 nm and fluorescence yield increases of 2−4-fold.

Fluorescence Quenching. The data thus far suggest that W alone experiences a somewhat hydrophobic environment in the cubic phase. However, the sense was that W, as a water-soluble zwitterionic amino acid, would spend a sizable fraction of its time in the aqueous channels of the mesophase. If so, its fluorescence should be quenchable by the water-soluble bromide in KBr. The original expectation was that quenching of W by bromide in the cubic phase would be similar to that in buffer. A quenching study was performed to test the hypothesis, and the results are shown in Figure 5. To our surprise, the cubic phase provided considerable protection for W against quenching by the water-soluble bromide ion. Thus, while 4 M KBr[5] quenched W fluorescence to the extent of ~75% in buffer, in the cubic phase, the corresponding value was <25%. Once again, these data

[5] The quenching study was performed under isoionic conditions where the relative amounts of KCl and KBr were changed.

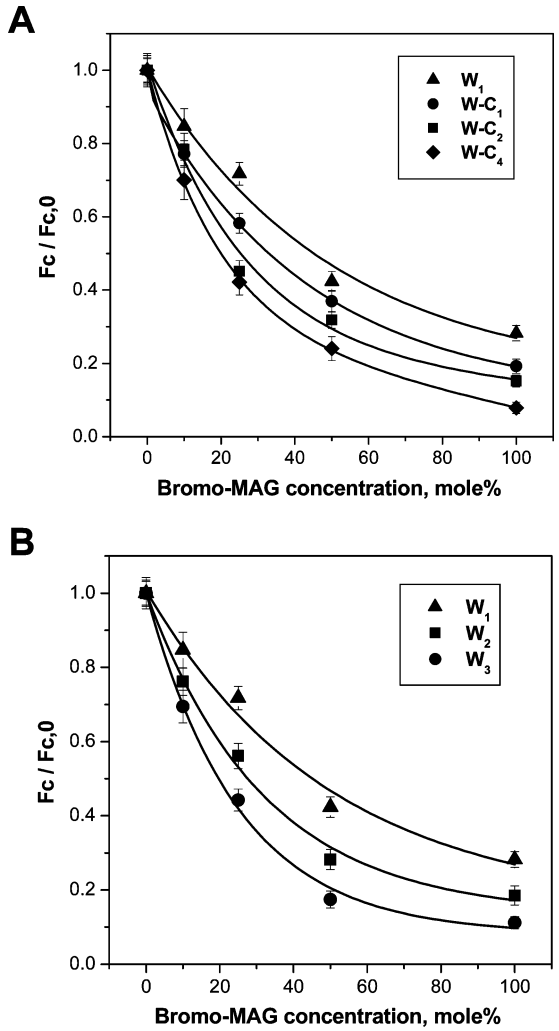

FIGURE 6: Fluorescence quenching of tryptophan and its alkyl (A) and peptide derivatives (B) in the cubic-*Pn*3*m* phase of hydrated monoolein at 20 °C. Bromo-MAG is the quenching lipid, and its concentration is expressed as mole % corresponding to 100 (mol of bromo-MAG)/[(mol of bromo-MAG) + (mol of monoolein)]. Flourescence data have been corrected for background fluorescence from SPP buffer and lipid and for the inner filter effect and have been normalized to the quencher-free ($F_{c,0}$) value. Data are shown as the average of at least three replicate sample preparations and fluorescence measurements. Error bars correspond to the standard deviation. Lines (double exponentials) have been drawn to guide the eye. Given the complex nature of the system under investigation where fluorophors are distributed to varying degrees between two very different environments, the bilayer interface and the aqueous solution, a more complete analysis was not considered informative at this stage and was not undertaken.

point to an environment for W that is partly interfacial and relatively inaccessible to water-soluble ions such as bromide.

The previous result suggested that if W spends a considerable fraction of its time at the membrane/aqueous interface, it should be accessible and in a position to be quenched by bromo-MAG. The latter monoacylglycerol has two bromine atoms at carbon atoms 9 and 10 in an 18 carbon acyl chain. In a previous study, almost complete quenching of the Ws in gramicidin, which are situated in the bilayer but close to the membrane/aqueous interface, was observed with bromo-MAG (*18*). The results of the current quenching study are shown in Figure 6A. Consistent with the hypothesis, considerable quenching of W—to the extent of ~70%—was observed in pure bromo-MAG.

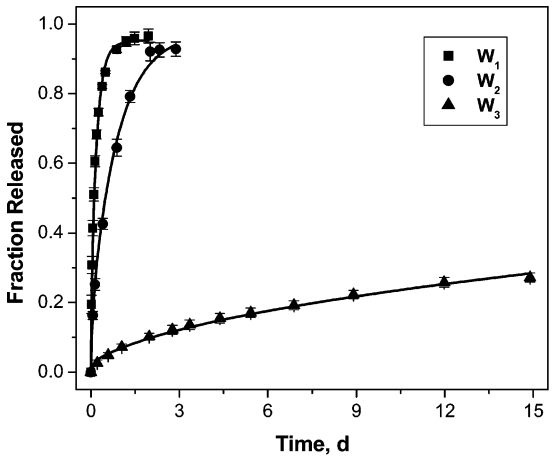

FIGURE 7: Release profiles of tryptophan peptides from the cubic-*Pn*3*m* phase of hydrated monoolein as a function of time at 20 °C. The solid lines represent fits to the release data based on average D_F and k values obtained from the diffusion model (Table S6). Error bars corresponding to the standard deviation are included for all data points and are based on triplicate measurements.

This result led to another hypothesis: that the W-alkyl series should show enhanced quenching with alkyl chain length. The data in Figure 6A support the proposal. As the chain length grew from 1 to 2 and 4 carbons, the extent and rate (as in change with quencher concentration) of quenching rose. These data are consistent with a W moiety that is anchored in the membrane more securely the longer the chain.

A similar hypothesis was advanced and confirmed for the W_n series as shown in Figure 6B. The more Ws in the peptide, the tighter the association with the membrane and the more rapid and complete the quenching.

In a final quenching study, the possibility of completely[6] eliminating W fluorescence was investigated by dispersing the amino acid in a cubic phase prepared using pure bromo-MAG and a concentrated solution of KBr. The data (Figure S3) show clearly that essentially complete quenching was achieved at 4 M bromide. Thus, presumably the bromine of bromo-MAG quenches the interfacial W, while the bromide ion takes care of W in the aqueous compartment.

Transport and Partitioning. One of the early indicators that W was partitioning at the membrane/aqueous interface of the cubic phase came from studies of its release from the mesophase (*11*). Upon loading with a W solution, release, recorded under infinite sink conditions, was rapid but incomplete with the last vestiges of W emerging on a much longer time scale. This bound W represented a small fraction of the total but was enough for a partition coefficient of 56 to be determined for the system (*11*). In the latter study, it was shown that release of the W—C_n series of additives was retarded in a way that reflected an enhanced partitioning into the cubic phase with increasing chain length.

In the current study, the release experiments were extended to include the W_n series with the expectation that the more Ws in the peptide the slower would be its release. The data in Figure 7 support this prediction. The release profiles have

[6] It is important to note that 100% quenching is not expected based on the work of Bolen and Holloway (*25*). In that study, a quenching efficiency of 82% was measured using a model system consisting of indole and 2,3-dibromobutane in methanol.

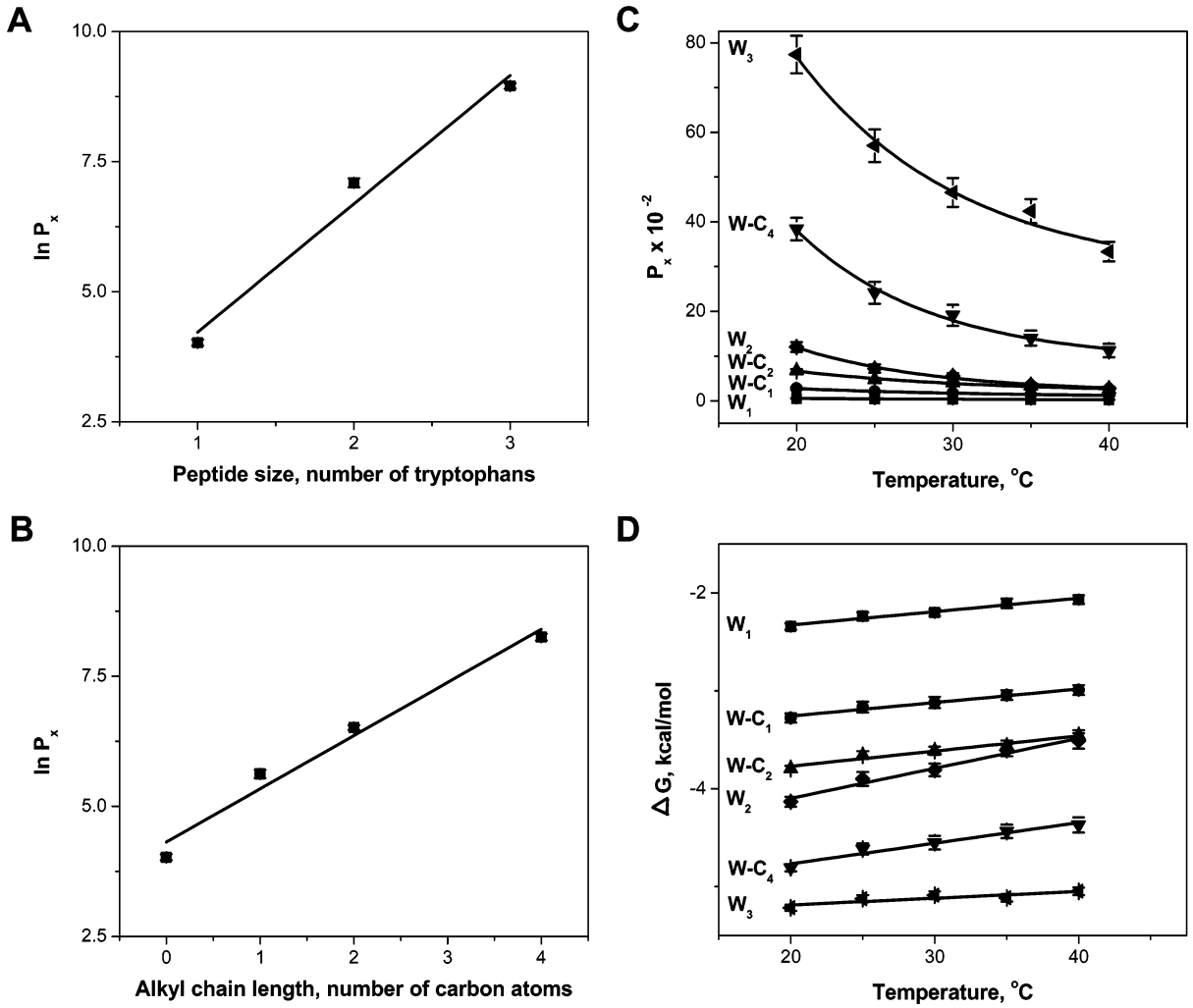

FIGURE 8: Temperature dependence of the partitioning of tryptophan and its derivatives into the cubic-*Pn*3*m* phase of hydrated monoolein. The partition coefficient, expressed in mole fraction units, is shown as a function of peptide size at 20 °C (A), alkyl chain length at 20 °C (B), and temperature (C). The free energy of partitioning is shown in panel D as a function of temperature and was calculated using eq 2 and the data in panel C. Data are shown as the average of at least three replicate sample preparations and partitioning measurements. Error bars correspond to the standard deviation. In some cases (A and B), the statistical error is smaller than the size of the symbols.

been analyzed to provide transport characteristics, diffusion coefficients, and rate constants (Table S6).

These data are consistent with the view that W and its derivatives are partitioning preferentially at the membrane/aqueous interface of the cubic phase. As noted, partition coefficient values have been determined for the W−C_n series on the basis of real-time uptake measurements (*11*). These have been extended to the W_n series (Table S6). As expected, P_χ rises exponentially with number of Ws in the peptide (Figure 8A). This is consistent with a cooperative interaction phenomenon as *n* goes from 1 to 2 to 4. A similar effect has been observed for peptides partitioning into glycerophospholipid vesicles (*26*).

That partitioning is reversible was investigated by first monitoring the uptake of one of the W derivatives, WW, into the cubic phase and then watching its release when the bathing solution was replaced with fresh buffer (see Materials and Methods). The data (not shown) are consistent with a process that is thermodynamically reversible. In a separate study, the same P_χ was observed for WW regardless of whether the determination was made as a release or an uptake measurement (data not shown). This demonstrates that the P_χ values reported are equilibrium values.

With a view to quantifying the relative contributions of enthalpy and entropy change to the free energy of partitioning, the temperature-dependence of the process was examined for W and its derivatives. The lowest temperature used in the study was 20 °C because below ~18 °C the cubic-*Pn*3*m* phase of fully hydrated monoolein is no longer stable (*16*). An upper limit of 40 °C was chosen to minimize the risk of W degradation at higher temperatures[7] and to retain the cubic-*Pn*3*m* phase. The thermodynamic data are presented in Figure 8 and Table 1. The results show that partitioning of W and the members of the W_n and W−C_n series has a large favorable ΔH and an unfavorable ΔS. The former is consistent with the so-called nonclassical hydrophobic effect documented originally by Huang and Carlton (*27*) and will be discussed.

Effect of Membrane Interfacial Properties on Partitioning. Thus far, a simple monoacylglycerol, monoolein, has been used to create the cubic phase for the partitioning studies. Our next objective was to determine if the partitioning

[7] Note that partition studies are conducted over a period of 4 days to ensure equilibration. It is for this reason that relatively low temperatures were used where W degradation does not occur.

Table 1: Thermodynamic Parameters Describing Tryptophan, Tryptophan Peptide, and Tryptophan Alkyl Ester Partitioning into Cubic Phase of Monoolein from Aqueous Medium

additives	ΔG (kcal/mol)[a]	ΔH (kcal/mol)	ΔS (cal/(mol K))
W_1	−2.3	−6.4	−13.7
$W-C_1$	−3.3	−7.3	−13.9
$W-C_2$	−3.8	−8.3	−15.5
$W-C_4$	−4.8	−10.9	−21.1
W_2	−4.1	−13.1	−30.7
W_3	−5.2	−7.2	−6.9
indole	−5.1	−10.0	−17.1

[a] Free energy values are reported at 293 K (20 °C).

Table 2: Effect of Glycerol, Urea, and Salt on Phase Properties and Partitioning of Tryptophanyl Tryptophan between the Aqueous Medium and the Cubic-*Pn*3*m* Phase of Monoolein at 20 °C

additive	additive concentrated (M)[a]	lattice parameter (Å)[b]	P_χ[c]
none	0.0	102	1204 ± 80
glycerol	6.0	92	127.3 ± 7.3
urea	8.0	127	450.8 ± 29.6
KCl	4.0	98	2950 ± 65

[a] Refers to the concentration of additive in the SPP buffer solution used to form the cubic phase. [b] The lattice parameter values reported are accurate to ±3 Å. [c] Average values are reported along with standard deviations ($n = 3$).

behavior was affected by altering the lipid profile and thus the interfacial properties of the hosting cubic phase. Accordingly, DOPC and DOPE were combined with monoolein and used to form the cubic phase. Care was taken not to add too much glycerophospholipid (≤20 mol %) that would destabilize the cubic phase (Table S3 and ref *17*). The data (Table S3) show convincingly that the partitioning of WW was unaffected by these chemically more heterogeneous lipids at loadings up to 18 mol %. This is so despite the fact that the curvature of the bilayer changes considerably and in opposite directions in PC and PE (Table S3), as discussed.

The peptides used in this study incorporate at least one peptide linkage. It was speculated that an amide functionality in the lipid at the bilayer interface would favor partitioning through complementary hydrogen bonding interactions. To test the hypothesis, monoolein was replaced by a phytaneamide lipid (PAL) where the linkage between the branched acyl chain and glycerol is of the amide type. Fully hydrated PAL forms the pure cubic-*Pn*3*m* phase at slightly above room temperature (unpublished data), and it has a lattice parameter similar to that of monoolein (Table S7). Therefore, to ensure that the PAL-based system was in the cubic phase throughout the study, measurements were carried out at 40 °C. The data show that WW partitions with respect to PAL in the same way that it does with respect to monoolein at the same temperature (Table S7). Neglecting the difference in the acyl chain character of PAL and monoolein, these results run counter to the hypothesis of a preferential association between the amide of the additive and that of the lipid at the bilayer interface.

Effects of Aqueous Channel Properties on Partitioning. The goal here was to explore the nature of the interaction between W derivatives and the membrane interface of the cubic phase. To this end, the aqueous phase used to create the mesophase was modified by the inclusion of KCl, urea, and glycerol. As before, care was taken to ensure that the cubic-*Pn*3*m* phase was stable under all such conditions as judged by small-angle X-ray diffraction. Partition measurements were performed with WW, which has a partition coefficient that is of intermediate value and thus maximally sensitive to effects on partitioning. The results show that partitioning can be modulated over a wide range depending on the water-soluble additive (Table 2). Thus, KCl enhanced WW partitioning by a factor of 2.5 while glycerol and urea lowered it in equal measure.

DISCUSSION

One of our long-term research objectives is to understand the mechanism by which membrane proteins crystallize in lipidic mesophases. The model for crystallogenesis upon which the work progresses suggests that the protein initially reconstitutes into the bilayer of the cubic phase and is free to diffuse therein (*10*). The model also requires precipitants, such as salts and an assortment of small organic molecules, to diffuse within the aqueous channels of the mesophase. In the process of characterizing these so-called transport properties, it was noted that W, while diffusing rapidly in the cubic phase, interacted weakly with the lipid bilayer (*12*). This came somewhat as a surprise given the highly curved nature of the membrane and the chemical simplicity and homogeneity of the bilayer/aqueous interface, the latter presumably coated with glycerol hydroxyls and ester functionalities. The current study is an extension of that earlier work. The focus here is on establishing the nature of the W-cubic phase interaction which, as discussed next, has implications for protein structure and function in membranes.

The current study began with a comparison of the spectroscopic properties of W in bulk aqueous solution and in the cubic phase. Electronic absorption spectroscopy revealed slight differences, suggesting that W in the mesophase was experiencing a different environment from that in bulk water. Fluorescence measurements showed that W was in a more hydrophobic space in the cubic phase as evidenced by the blue shift and elevated fluorescence yield. These data are consistent with the original view that W does indeed associate with the bilayer interface of the cubic phase. The idea was further corroborated by studies showing that bromide ions were incapable of quenching the fluorescence of W in the mesophase to the same extent as it did in bulk water. This was interpreted as indicating that W was sequestered, to a degree, in the interface and was fractionally inaccessible to the bromide for interaction and quenching. However, essentially complete elimination of W fluorescence was brought about when the quenching by bromide in the aqueous compartment was augmented by quenching in the apolar region of the membrane by way of the lipid, bromo-MAG.

Taken together, these data make a case for W/cubic phase bilayer interaction. However, the evidence was not as strong as we would have liked. For example, a partitioning value of 56, while measurable, is still small. What we set out to do therefore was to test the hypothesis that alkylating W should amplify the effects seen with W alone. Further, the longer the chain, the more W would become anchored in the bilayer and the more obvious the effects reflecting bilayer association would be. The results obtained fit the hypothesis.

Blue shifts and fluorescence yields were magnified with the alkylated Ws in a chain length-dependent manner. Quenching was more extreme in the longer chained alkyl Ws.

In an effort to explore the interaction of W with the cubic phase membrane a little further, a different strategy was taken with the W_n peptide series. The reasoning was that if W in isolation (W_1) interacted weakly, then a cooperative interaction should be seen with W dipeptides (W_2) and tripeptides (W_3). This W_n series study was also motivated by the nonuniform distribution of Ws in integral membrane proteins highlighted originally by Diessenhofer and Michel (*1*). The electronic absorption, fluorescence, and quenching data for the W_n series were consistent with the prediction. Further, transport of W_3 in the cubic phase was considerably slower than that of W_2 and W_1, as expected. This was reflected in the exponentially rising bilayer partitioning recorded for the W_n series as n increased.

Thermodynamics. It has long been observed that partitioning of amphiphilic and apolar substances into bilayers is distinctly different from their partitioning into a bulk apolar solvent (*27*−*30*). The fact that the bilayer is part of a liquid crystalline phase with order intermediate between that of a crystalline solid and an isotropic liquid, the latter observation should not come as a surprise. The bilayer thus has a very distinct structure and dynamic characteristics that set it apart from a liquid hydrocarbon. In contrast to a partitioning that is entropy driven, partitioning into a bilayer is dominated by a very favorable enthalpy change. As yet, the origin of the latter has not been explained satisfactorily.

In the current study, we set out to explore the contributions of enthalpy and entropy changes to the partitioning free energy of W and its derivatives in the lipidic cubic phase. In the discussion that follows, the assumption is made that ΔH and ΔS are temperature invariant in the narrow 20 to 40 °C range examined. Our first observation was that partitioning of all Ws studied dropped with increasing temperature (Figure 8C). This dependence gave rise to an unfavorable ΔS (Table 1) but was countered by a large negative ΔH that dominated. The latter is the hallmark of the so-called nonclassical hydrophobic effect (*28*).

These results are similar to those obtained with large unilamellar phospholipid vesicles where the W analogues investigated included indole, *N*-methylindole, and 3-methylindole (*30*). The only difference was in the sign of ΔS, which is negative for W and its derivatives (this study) and positive in the work on W analogues. To make possible a comparison for a common additive, the cubic phase measurement was repeated with indole. Again, the data show that while the sign of ΔG and ΔH remain the same for the mesophase and vesicle systems, it differs in the case of ΔS (Table 1). It is not clear to what these disparate behaviors can be ascribed. However, it is worth noting that the two systems have opposite thermal surface area expansivities. In the case of vesicles, the area per headgroup rises with temperature. The cubic phase, in contrast, loses water upon heating (Figure S1), which leads to a reduction in interfacial surface area.

Factors That Affect Partitioning. Urea. Measurements were performed in 8 M urea where one in every seven or eight lyotrope molecules is urea. Urea is a small molecule bristling with both hydrogen bond donors and acceptors. It is used to unfold and to solubilize proteins. Mass action likely plays a role in the process where intramolecular hydrogen bonding is overwhelmed by intermolecular hydrogen bonding to urea, especially at high concentrations (*31*). We speculated that it would have a similar effect on WW. The latter has hydrogen bond donors and acceptors along its main chain backbone and a donor at the indole nitrogen. Hydrogen bonding to the backbone and especially to the indole nitrogen should favor partitioning into the polar aqueous compartment and away from the bilayer interface. This view is supported by the data where P_χ was reduced by a factor of ∼2.7 in the presence of urea (Table 2). While urea also lowers interfacial curvature (Table S5), this is unlikely to play a major role here because PC, which has a similar effect on curvature, did not alter partitioning (Table S3).

KCl. Partitioning measurements were performed in the presence of 4 M KCl. This creates a highly polar aqueous compartment within the cubic phase that has approximately one ion for every seven or eight water molecules. The net effect was to raise the partitioning of WW at the bilayer interface by a factor of ∼2.5 as compared to that of the low ionic strength reference condition (Table 2). The result makes good sense. While WW is zwitterionic with no net charge under conditions of measurement, the polar part of the molecule should not interact electrostatically with the neutral interface provided by the esterified glycerol headgroup of monoolein. Thus, the salt effect is not expected to be large on this account. However, the indole side chain of WW has two apolar benzene rings. The high polarity of the aqueous medium in the presence of 4 M KCl is therefore likely to drive this part of WW toward the bilayer interface where the rings can find respite in or close to the hydrocarbon interior of the membrane.

Glycerol. Glycerol was included in this study as a control substance. From previous work (unpublished) we had shown that the cubic phase tolerated surprisingly large amounts of the water-soluble polyol without undergoing a phase change. The only effect seen up to 70% (w/w) glycerol was a reduction in the lattice parameter of the cubic phase by 10 Å from an initial value of 103 Å in water. And since DOPE, which also reduces the lattice parameter, had no effect on partitioning (Table S3), our expectation was that glycerol would similarly be innocuous. However, the data show that it dramatically reduced the interfacial partitioning of WW (Table 2). How it achieved this effect is a matter of speculation. One possibility is that it interacts with WW in such a way as to raise its aqueous solubility. The fact that the glycerol molecule has an apolar surface that could favorably interact with the indole rings of WW is consistent with this view. Another is that it induces formation of a tightly packed bilayer interface of such density as to resist the partitioning of the dipeptide.

Advantages of the Cubic Phase. The cubic phase is well-suited to partitioning studies of the type reported here. To begin with, the cubic phase at 20 °C is maximally hydrated at about 40% (w/w) water (Figure S1). This means that a bolus of the cubic phase remains in equilibrium with a bulk aqueous solution at ≥40% (w/w) hydration. Further, since the cubic phase is extremely viscous and sticky, the mesophase stays put where it is placed. This obviates the need for a membrane to separate the source (aqueous medium) and the sink (cubic phase) in transport and partitioning measurements. These two features facilitate the direct and

continuous photometric assay of such processes when carried out in a cuvette, as in the current study. Since the lipid used in this investigation, monoolein, imbibes less than half its mass as water at full hydration, the cubic phase is highly concentrated in lipid (~2 M) and thus membrane. Accordingly, because the sink is so concentrated, the sensitivity of the partitioning assay is enhanced. This enables the characterization of materials with low partition coefficients. W is a case in point (Table S6), and the enhanced sensitivity obviates the need to substitute it with apolar analogues having higher bilayer partitioning. The cubic phase is intrinsically porous (*11*, *12*) with both sides of the bilayer accessible to the partitioning molecule (Figures 2 and 7). This is in contrast to liposomes where typically just one side of the membrane is available for interaction. The cubic phase also has the advantage of being optically isotropic. Thus, transparent samples can be prepared that lend themselves to direct spectroscopy (*18*, *32*).

Cubic Phase as a Model Membrane System. The cubic phase is a bicontinuous mesophase with approximately half its mass in the form of a lipid leaflet and the other half aqueous channel. A characteristic of the cubic phase bilayer that sets it apart from most biomembranes is its curvature. However, high curvature is also to be found in natural membranes. Secretory vesicles, retinal disks, inner mitochondrial and thylakoid membranes, cubic membranes, and cavaeoli are examples. Nevertheless, it is appropriate to examine the relevance of the cubic phase as a model membrane system, despite its high curvature.

The data reported herein indicate that in the range studied, curvature had little effect on partitioning. Thus, the glycerophospholipid PC, which lowers it, and PE, which elevates it, had no impact on the partition coefficient of WW (Table S3).

The bulk of the work done with model membranes makes use of uni- and multilamellar vesicles. Small unilamellar vesicles (SUV), while they have advantages, are not considered as desirable as their large unilamellar vesicle (LUV) counterpart because of intrinsic instability and high curvature. Further, very small vesicles have a host of physical−chemical properties, including partition coefficients (*8*), that are different from large vesicles. In the current study, we measured the partitioning of indole into cubic phase membranes that enabled a comparison with literature values for LUVs. As noted, ΔG and ΔH for the cubic phase and LUVs have the same sign, although they differ in absolute values (Table 1). In this regard then, the two systems mimic one another, and the curved bilayer of the cubic phase is analogous to its more planar counterpart in the vesiculated system. A difference does emerge in the entropy change associated with partitioning in that it is negative for the mesophase and positive for vesicles (Table 1). Under conditions of measurement however, the disparity is irrelevant as far as partitioning is concerned since it is the favorable enthalpy change that dominates the process.

While the previous discussion contrasts the mesophase and vesicle systems with a focus on curvature, it is important to bear in mind that the lipids used in the two studies are distinctly different. In one it is a diacyl chain glycerophospholipid. In the other, it is a monoacylglycerol. The disparate behaviors therefore must be evaluated at least in light of the contrasting chemical and dynamical properties of the respective polar/apolar interfaces.

Regardless of whether the cubic phase is a good model membrane system, the studies described herein were performed to better characterize the cubic phase that is proving to be invaluable in membrane protein crystallogenesis (*2*, *10*, *33*, *34*) and in controlled uptake and release applications (*11*, *12*).

Relevance to Inclusion Body Reconstitution, Refolding, and Crystallization. The overexpression of membrane proteins often leads to the production of inclusion bodies. These can be solubilized and refolded in detergent solution for use in crystallogenesis. We have proposed using solubilized inclusion bodies for direct in meso crystallization (*10*). The idea is as follows. The protein, dissolved in a concentrated denaturant (urea, for example) solution, is used to form the cubic phase. Upon incubation with excess buffer, the urea rushes out of the porous mesophase, and the protein begins to refold. Since it is essentially trapped in the narrow aqueous confines of the cubic phase, the protein is only angstroms away from the lipid bilayer and spontaneously reconstitutes into it. The protein-loaded mesophase can then be used directly in in meso crystallogenesis.

Our finding that urea lowers the affinity of WW for the cubic phase bilayer further rationalizes the previous proposal. Consider for a moment a short β-barrel membrane protein with Ws in its sequence, one that forms inclusion bodies. The urea-solubilized protein will reside in the aqueous channel of the cubic phase upon mesophase formation. As urea exits the cubic phase upon bathing in buffer, the natural tendency of W to interact with the bilayer interface will become more pronounced. This will pin the protein to the interface preferentially at sites in the sequence where W is located. In turn, it will bring adjacent stretches of peptide into close proximity with the bilayer interface. Since the protein is predominantly a β-sheet, this proximity may facilitate orientation of the peptide there with side chains of residues n, $n + 2$, $n + 4$, ... facing in one direction; toward the bilayer interior, for example. Then, residues $n + 1$, $n + 3$, $n + 5$, ... will face the aqueous phase. Such oriented amphiphilic strands would be free to diffuse on the surface of the bilayer and to find partners with which to form amphiphilic β-sheets. However, a pair of strands in a β-sheet conformation at the interface would likely introduce a defect in the leaflet on which it sits, causing the lipids to splay apart. This may trigger a flipping of the duplex across the bilayer, taking water with it. In a cooperative manner, other nearby strand duplexes and possibly triplets would join in the process, leading to the formation of a transmembranal β-barrel. The Ws, if suitably located in the sequence, may anchor the two ends of the barrel in the membrane and impact on its orientation and activity therein. Subsequent annealing might be necessary to enable the protein to assume its lowest energy conformation and to become fully active. The relevance of this model to membrane protein insertion and folding should be obvious.

The previous rationalization has been presented in the context of how urea may facilitate the reconstitution process. The effects seen with high salt, described previously, might be used to advantage here too. KCl was shown to increase the partitioning of WW to the interface. Thus, the experiment could be done where the bathing solution has a high salt concentration. This would serve double-duty: it would act as a sink into which urea would diffuse from the cubic phase

at the same time that salt diffuses in. The cubic phase would experience a falling urea concentration and a rising salt concentration, both of which will serve to anchor W at the interface and assist in the refolding and reconstitution process.

Impact on Membrane Anchoring, Orientation, and Fusion. The observations regarding aromatic residue stratification at the bilayer polar/apolar interface of membrane proteins can be interpreted in light of the findings reported herein. Partitioning was shown in the current study to rise exponentially with the number of contiguous Ws in the peptide in the range studied. Thus, the ΔG per residue is additive. In the case of integral membrane proteins and peptides, the aromatic residues at the interface may not necessarily follow closely in sequence but are often neighboring in the folded structure (Figure 1). This spatial proximity is analogous to the W_n series studied here and contributes to defining the interface and to orienting the protein in the membrane between the two interfaces that much more exactly. Since the measured ΔG is large, the energy cost of a protein undergoing a conformational and/or orientation change that repositions the Ws from their preferred location at the interface can be very high. In this way then Ws, and other aromatics, particularly tyrosine, at the interface may play an important role in regulating protein function and distribution in membranes. The thicknesses of membranes within the cell differ (*35*). As the database of membrane protein structures grows (*2*), it will be interesting to see if the distance separating the band of aromatics at the bilayer interface correlates with membrane location of the protein within the cell. In addition to an anchoring role within its own membrane, it seems reasonable that strings of Ws and other aromatics could bind to free vesicles and to other membranes within and outside the cell, thereby contributing to intracellular trafficking and membrane fusion.

As noted in the introductory paragraphs, the first high-resolution crystal structure of a membrane protein served to highlight the stratification of aromatic residues at the putative polar/apolar interface (*1*). However, in that work, lipid molecules were not identified, and so the nature of the implied interaction between aromatics and membrane lipid could not be explored. Since that time, several membrane protein structures have appeared in which lipids are seen clearly. A survey of entries in the Membrane Protein Data Bank (http://www.mpdb.ul.ie) has identified 59 such records corresponding to 20 distinct protein types. In several of these, interfacial tryptophans make contact with lipid molecules in ways that are consistent with the results of the current study. One such example, the mitochondrial ADP/ATP carrier, is illustrated in Figure 1 (panel B4). In this case, tryptophan at position 70 in the protein (Trp70) sits next to a cardiolipin molecule with its flat indole ring surface parallel to the long axis of one of the lipid acyl chains. As expected, its peptide end is adjacent to one of the phosphoglyceryl moieties in the lipid headgroup. It should be pointed out that instances of crystal structures with interactions of the type just described are not common. However, this does not necessarily mean that such interactions are rare. Rather, it likely reflects natural disorder in the lipid that prevents it being seen crystallographically and/or loss of lipid in the purification and crystallization processes.

CONCLUSION

Tryptophan was shown to interact weakly with the highly curved monoolein bilayer of the cubic phase. Its alkyl ester and peptide derivatives interacted more strongly and did so in a length-dependent way. In all cases, the association was driven by a favorable enthalpy change. Electronic absorption and fluorescence spectroscopic signatures were consistent with an interaction that placed the indole ring of tryptophan in a more hydrophobic environment and presumably at the polar/apolar interface of the membrane. The interfacial location was further verified by fluorescence quenching from both the aqueous polar and the bilayer apolar compartments. Transport measurements supported the view that partitioning into the interface is dynamic and dependent on the number of tryptophans in the case of the peptide derivatives. The degree of interaction could be controlled by altering the character of the aqueous medium in the cubic phase. Thus, glycerol and urea lowered the affinity, while salt enhanced it. In contrast, the interfacial properties of the bilayer, including its curvature, could be modified by the inclusion of phosphatidylcholine and phosphatidylethanolamine without effect on partitioning. Thus, the chemical complexity and heterogeneity of the interface appears to contribute little to the partitioning phenomenon in the range studied.

The effects of urea and salt on tryptophan partitioning described in this paper suggest a protocol for the in meso reconstitution and crystallization of membrane proteins that start out as inclusion bodies.

The results obtained with the tryptophan peptides highlight the benefit of having multiple adjacent aromatic residues in close proximity in terms of locking the protein at the bilayer interface. This has implications for protein orientation, distribution, and function in and on membranes and may play a role in cellular trafficking and membrane fusion. The cubic phase offers a number of distinct advantages as a system with which to perform partitioning studies and as a model membrane.

ACKNOWLEDGMENT

The authors thank V. Cherezov, J. Clogston, and J. Lyons for valuable discussions.

SUPPORTING INFORMATION AVAILABLE

Additional information regarding X-ray diffraction and spectroscopic, partitioning, and transport characteristics of the system. This material is available free of charge via the Internet at http://pubs.acs.org.

REFERENCES

1. Deisenhofer, J., and Michel, H. (1989) Nobel lecture. The photosynthetic reaction centre from the purple bacterium *Rhodopseudomonas viridis*, *EMBO J. 8*, 2149−2170.
2. Raman, P., Cherezov, V., and Caffrey, M. (2005) The Membrane Protein Data Bank, *Cell Mol. Life Sci. 63*, 36−51.
3. Lee, A. G. (2002) Ca^{2+}-ATPase structure in the E1 and E2 conformations: mechanism and helix−helix and helix−lipid interactions, *Biochim. Biophys. Acta 1565*, 246−266.
4. Kachel, K., Asuncion-Punzalan, E., and London, E. (1995) Anchoring of tryptophan and tyrosine analogues at the hydrocarbon−polar boundary in model membrane vesicles: parallax analysis of fluorescence quenching induced by nitroxide-labeled phospholipids, *Biochemistry 34*, 15475−15479.

5. Yau, W. M., Wimley, W. C., Gawrisch, K., and White, S. H. (1998) The preference of tryptophan for membrane interfaces, *Biochemistry 37*, 14713−14718.
6. Killian, J. A., and von Heijne, G. (2000) How proteins adapt to a membrane−water interface, *Trends Biochem. Sci. 25*, 429−434.
7. de Planque, M. R., Bonev, B. B., Demmers, J. A., Greathouse, D. V., Koeppe, R. E., II, Separovic, F., Watts, A., and Killian, J. A. (2003) Interfacial anchor properties of tryptophan residues in transmembrane peptides can dominate over hydrophobic matching effects in peptide−lipid interactions, *Biochemistry 42*, 5341−5348.
8. White, S. H., and Wimley, W. C. (1999) Membrane protein folding and stability: physical principles, *Annu. Rev. Biophys. Biomol. Struct. 28*, 319−365.
9. Landau, E. M., and Rosenbusch, J. P. (1996) Lipidic cubic phases: a novel concept for the crystallization of membrane proteins, *Proc. Natl. Acad. Sci. U.S.A. 93*, 14532−14535.
10. Caffrey, M. (2003) Membrane protein crystallization, *J. Struct. Biol. 142*, 108−132.
11. Clogston, J., Craciun, G., Hart, D. J., and Caffrey, M. (2005) Controlling release from the lipidic cubic phase by selective alkylation, *J. Controlled Release 102*, 441−461.
12. Clogston, J., and Caffrey, M. (2005) Controlling release from the lipidic cubic phase. Amino acids, peptides, proteins, and nucleic acids, *J. Controlled Release 107*, 97−111.
13. Cheng, A., Hummel, B., Qiu, H., and Caffrey, M. (1998) A simple mechanical mixer for small viscous lipid-containing samples, *Chem. Phys. Lipids 95*, 11−21.
14. Qiu, H., and Caffrey, M. (1998) Lyotropic and thermotropic phase behavior of hydrated monoacylglycerols: structure characterization of monovaccenin, *J. Phys. Chem. B 102*, 4819−4829.
15. Briggs, J. (1994) The phase behavior of hydrated monoacylglycerols and the design of an X-ray compatible scanning calorimeter. Ph.D. Thesis, The Ohio State University, Columbus, OH.
16. Qiu, H., and Caffrey, M. (2000) The phase diagram of the monoolein/water system: metastability and equilibrium aspects, *Biomaterials 21*, 223−234.
17. Cherezov, V., Clogston, J., Misquitta, Y., Abdel-Gawad, W., and Caffrey, M. (2002) Membrane protein crystallization in meso: lipid type-tailoring of the cubic phase, *Biophys. J. 83*, 3393−3407.
18. Liu, W., and Caffrey, M. (2005) Gramicidin structure and disposition in highly curved membranes, *J. Struct. Biol. 150*, 23−40.
19. Lakowicz, J. R. (1983) *Instrumentation of fluorescence spectroscopy*, Vol. 2, Plenum Press, New York.
20. Engstrom, S., Norden, T. P., and Nyquist, H. (1999) Cubic phases for studies of drug partition into lipid bilayers, *Eur. J. Pharm. Sci. 8*, 243−254.
21. *CRC Handbook of Chemistry and Physics*, 63rd ed., CRC Press, Inc., Boca Raton, FL.
22. Cherezov, V., Qiu, H., Pector, V., Vandenbranden, M., Ruysschaert, J. M., and Caffrey, M. (2002) Biophysical and transfection studies of the diC(14)-amidine/DNA complex, *Biophys. J. 82*, 3105−3117.
23. Caffrey, M. (1985) Kinetics and mechanism of the lamellar gel/lamellar liquid crystal and lamellar/inverted hexagonal phase transition in phosphatidylethanolamine: a real-time X-ray diffraction study using synchrotron radiation, *Biochemistry 24*, 4826−4844.
24. Ricci, R. W., and Nesta, J. M. (1976) Inter- and intramolecular quenching of indole fluorescence by carbonyl compounds, *J. Phys. Chem. 80*, 974−980.
25. Bolen, E. J., and Holloway, P. W. (1990) Quenching of tryptophan fluorescence by brominated phospholipids, *Biochemistry 29*, 9638−9643.
26. Ladokhin, A. S., and White, S. H. (2001) Protein chemistry at membrane interfaces: nonadditivity of electrostatic and hydrophobic interactions, *J. Mol. Biol. 309*, 543−552.
27. Huang, C., and Charlton, J. P. (1971) Studies on phosphatidylcholine vesicles. Determination of partial specific volumes by sedimentation velocity method, *J. Biol. Chem. 246*, 2555−2560.
28. Seelig, J., and Ganz, P. (1991) Nonclassical hydrophobic effect in membrane binding equilibria, *Biochemistry 30*, 9354−9359.
29. Tanford, C. (1980) *The Hydrophobic Effect: Formation of Micelles and Biological Membranes*, 2nd ed., Wiley, New York.
30. Wimley, W. C., and White, S. H. (1993) Membrane partitioning: distinguishing bilayer effects from the hydrophobic effect, *Biochemistry 32*, 6307−6312.
31. Timasheff, S. N., and Xie, G. (2003) Preferential interactions of urea with lysozyme and their linkage to protein denaturation, *Biophys. Chem. 105*, 421−448.
32. Caffrey, M. (2000) A lipid's eye view of membrane protein crystallization in mesophases, *Curr. Opin. Struct. Biol. 10*, 486−497.
33. Misquitta, L. V., Misquitta, Y., Cherezov, V., Slattery, O., Mohan, J. M., Hart, D., Zhalnina, M., Cramer, W. A., and Caffrey, M. (2004) Membrane protein crystallization in lipidic mesophases with tailored bilayers, *Structure 12*, 2113−2124.
34. Cherezov, V., Clogston, J., Papiz, M. Z., and Caffrey, M. (2006) Room to move: crystallizing membrane proteins in swollen lipidic mesophases, *J. Mol. Biol. 357*, 1605−1618.
35. Mitra, K., Ubarretxena-Belandia, I., Taguchi, T., Warren, G., and Engelman, D. M. (2004) Modulation of the bilayer thickness of exocytic pathway membranes by membrane proteins rather than cholesterol, *Proc. Natl. Acad. Sci. U.S.A. 101*, 4083−4088.

BI0608414